frontiers | Frontiers in Materials

TYPE Original Research
PUBLISHED 02 September 2024
DOI 10.3389/fmats.2024.1445848

OPEN ACCESS

EDITED BY
Lu Ke,
Guangxi University, China

REVIEWED BY
Zhi-Wei Yan,
Beijing University of Technology, China
Li Xiaoda,
Guangzhou University, China

*CORRESPONDENCE
Dong Guo,
dong.gzhu@gzhu.edu.cn

RECEIVED 08 June 2024
ACCEPTED 17 June 2024
PUBLISHED 02 September 2024

CITATION
Liu Y, Huo S, Fu J, Shi T and Guo D (2024), Dynamic properties of CO_2-cured foam concrete at different loading rates: Effect of the foam admixtures and addition of polypropylene fiber.
Front. Mater. 11:1445848.
doi: 10.3389/fmats.2024.1445848

Dynamic properties of CO_2-cured foam concrete at different loading rates: Effect of the foam admixtures and addition of polypropylene fiber

Yunlin Liu[1,2], Shangwei Huo[2], Jiali Fu[2], Tingbo Shi[3] and Dong Guo[4]*

[1]Prefabricated Building Research Institute of Anhui Province, Anhui Jianzhu University, Hefei, China, [2]College of Civil Engineering, Anhui Jianzhu University, Hefei, China, [3]China Construction Third Bureau First Engineering Co., Ltd., Wuhan, China, [4]School of Civil Engineering and Transportation, Guangzhou University, Guangzhou, China

This paper investigated the dynamic mechanical properties of CO_2-cured foam concrete under varying conditions, focusing on the effects of foam admixture and fiber reinforcement. The study tends to enrich the knowledge regarding the performance of CO_2-cured foam concrete under different loading rates, especially in relation to density and matrix strength. The foam admixture of the specimens ranges from 26% to 55%, achieving density from 600 kg/m^3 to 1,000 kg/m^3. The specimens were loaded at strain rates from 80 s^{-1} to 398 s^{-1}. Experimental results revealed the dynamic elastic modulus, dynamic compressive strength, and Dynamic Increase Factor (DIF) showed a strong correlation with the foam admixture and density. In addition, the incorporation of polypropylene (PP) fibers effectively improved the mechanical behavior of the foam concrete, achieving up to a 17% increase in dynamic compressive strength. This comprehensive analysis highlights the critical role of foam admixture and fiber reinforcement in determining the dynamic properties of CO_2-cured foam concrete and provides valuable insights for optimizing the dynamic performance of foam concrete in various construction applications.

KEYWORDS

foam concrete, CO_2-curing, polypropylene fiber, SHPB, dynamic impact

1 Introduction

Foam concrete has been recognized as a popular material in the construction field due to its exceptional properties, including excellent heat insulation, fire resistance, and lightweight characteristics. Its application has recently expanded in aircraft arresting systems and military arresting engineering, primarily because of its superior cushioning and energy-absorbing characteristics (Liu et al., 2007). Foam concrete can be utilized independently or in combination with other materials such as ordinary concrete (Wang et al., 2015; Yang et al., 2020), light steel and calcium silicate board (Li et al., 2022), and carbon fiber-reinforced polymers (Wang et al., 2019; Yan et al., 2021) for energy absorption purposes.

CO_2 curing can enhance the strength of cementitious materials, especially at an early stage, achieving a reaction rate even comparable to the autoclave curing (Shi et al., 2012).

It is because cement primarily comprises tricalcium silicate (C_3S), dicalcium silicate (C_2S), tricalcium aluminate (C_3A), and tetracalcium aluminoferrite (C_4AF), all of which react with CO_2. Thus, the CO_2 curing technology for concrete leverages the carbonation characteristics of these major cement constituents (Shi et al., 2017). In the early stages of hydration, calcium silicate reacts with water to form calcium hydroxide ($Ca(OH)_2$) and calcium silicate hydrate (C-S-H) gel, which contributes to early strength development and creates an alkaline environment. Shi Caijun et al. (Rostami et al., 2012) examined the effects of different CO_2 curing variables on concrete performance. In comparison to autoclaved aerated concrete, CO_2 mineralization curing requires only 4–8 h to achieve the same strength that autoclaved curing reaches in 18–24 h. Accelerating the curing rate can decrease the casting period and improve construction efficiency (Deng et al., 2024). In the authors' previous studies (Liu et al., 2023a), a novel technique was developed for introducing CO_2 into the babbles, to achieve CO_2 curing in foam concrete.

Extensive studies have focused on the properties of foam concrete under static loading conditions (Liu et al., 2023a; Liu et al., 2023b). These studies have found that the properties of foam concrete are determined by both the pore characteristics and the strength of the cementitious matrix. The dynamic properties of foam concrete, however, differ significantly from those observed under quasi-static loading. As the strain rate increases, the failure mode transitions from uniform compaction failure to layer-by-layer collapse failure (Huang et al., 2020).

The pores in foam concrete influence the propagation path of the stress wave; when the stress wave encounters the free surface of a pore, it undergoes multiple refractions, reflections, and diffractions (Wang et al., 2021). Additionally, the plastic compression of pore collapse is a primary factor in stress wave attenuation within foam concrete (Blanc et al., 2021). Under dynamic loading, the failure process of foam concrete can be categorized into three stages: the elastic deformation stage, the crushing stage, and the post-failure stage (Blanc et al., 2021), while the stress-strain curve of foam concrete exhibits a strain plateau, facilitating its significant energy absorption capacity. Furthermore, the fractal dimension of impact load damage is found to be proportional to the strain rate, indicating that higher strain rates resulted in greater overall damage (He et al., 2019; Guo et al., 2020; Feng et al., 2020). In addition, the critical strain, compressive strength, and toughness of Large-Rupture-Strain (LRS) FRP-confined concrete specimens increase with increasing strain rate within the investigated strain rate range of 150 s^{-1} to 260 s^{-1} under impact loading (Yan et al., 2021).

Zheng and Jones (2013) conducted low-speed impact tests on ordinary commercial foamed concrete, revealing that the energy absorption capacity of various foamed concretes ranged from 4 to 15 MJ/m^3. Notably, foamed concrete with a water-cement ratio between 0.6 and 0.7 exhibited the most effective energy absorption (Zheng and Jones, 2013). Based on these test results, five distinct failure modes were proposed to describe the failure process of foam concrete. Furthermore, to investigate the relationship between the damage of porous materials and energy absorption under dynamic loads, Feng et al. (2022) conducted dynamic mechanical experiments on three types of foam concrete with varying densities, i.e., pore characteristics. The study found that the fractal dimension increased as a quadratic function with the rise in strain rate and demonstrated a transitional behavior at a strain rate of 140 s^{-1}.

The energy absorption capacities of foam concrete can also be modified by adding materials to the cementitious matrix, such as rubber (Lu et al., 2022) and fibers (Ma et al., 2023). Different rubber content has a certain effect on the dynamic mechanical properties of foamed concrete under impact load: at the same strain rate, the dynamic compressive strength of high rubber content foamed concrete is lower than that of low rubber content foamed concrete. Within an appropriate dosage range, the addition of rubber can improve the energy absorption capacity of foamed concrete, thereby enhancing the impact resistance of rubber foamed concrete (Lu et al., 2022). Furthermore, adding fibers to the foam concrete matrix can improve its toughness (Ma et al., 2023) due to the bridging effect of the fibers within the cementitious matrix (Guo et al., 2022; Guo et al., 2023). Additionally, the polypropylene fiber content is linearly related to the density and toughness of foamed concrete (Gökçe et al., 2023).

Based on the above literature, it is evident that the properties of foam concrete can be modified by altering the characteristics of the cementitious matrix or the pore characteristics. These modifications can be achieved through various strength enhancement methods, such as fiber reinforcement, CO_2 curing, or adjusting porosity. However, there is a gap in understanding the properties of CO_2-cured foam concrete under different loading rates, particularly concerning variations in porosity (density) and matrix strength. Therefore, this study aims to investigate the rate-dependent behavior of foam concrete with different foam admixtures and the presence or absence of PP fiber additions.

2 Test overview

In this study, a combination of CO_2 curing and fiber reinforcement is employed to enhance the dynamic properties of the cementitious matrix. CO_2 gas is introduced into the pores of the foam concrete during the physical foaming process, while PP fibers are incorporated into the cementitious matrix. The dynamic properties are then tested using the Split Hopkinson Pressure Bar (SHPB) equipment at different strain rates.

2.1 Test program

The cement used in the specimen is ordinary silicate cement (OPC) produced by Weiden Cement Group Limited Liability Company, with a strength grade of 52.5, and all the technical indexes comply with the GB175-2007 standard. Fly ash is the fine particle powder collected in the flue gas after the combustion of pulverized coal, which can get the specified fineness after grinding and processing. This test uses the fly ash produced by the Henan Yulian Energy Group Power Plant. Silica ash, also known as micro-silica powder, is a powder product with SiO_2 as the main component collected in the flue during industrial smelting of ferrosilicon alloy. In this test, the silica ash produced by Henan Platinum Run Foundry Material Co. The chemical compositions of cement, fly ash, and silica fume are shown in Table 1. The gas used in this test was industrial-grade CO_2 gas, produced by Anhui Hefei Shenqi Gas Co. with a purity of 99.5%. The length of pp fiber used

TABLE 1 The chemical compositions of cement, fly ash, and silica fume (%).

	CaO	SiO_2	Al_2O_3	Fe_2O_3	MgO	SO_3	K_2O	Na_2O
Cement	62.30	20.80	4.88	3.14	3.72	2.63	-	-
Fly ash	4.01	50.67	30.83	6.07	0.92	1.68	2.85	-
Silica fume	0.39	96.2	0.61	0.32	1.12	-	0.11	0.75

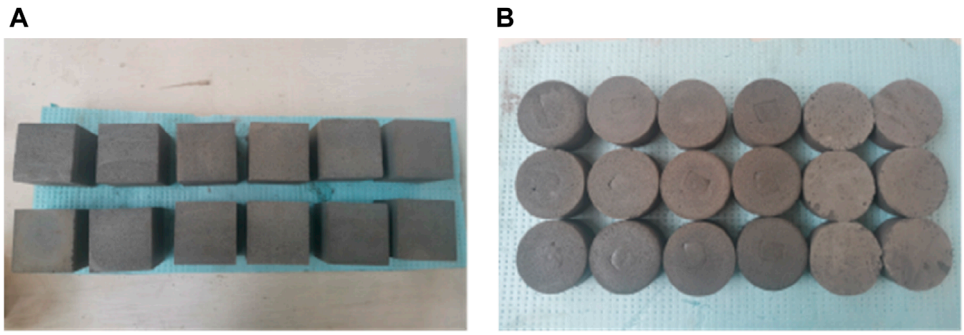

FIGURE 1
Pictures of specimens: **(A)** cubic specimen; **(B)** cylindrical specimen diagram.

in the experiment was 6 mm, the tensile strength was 556.9 MPa, and the elongation at break was 29.8%.

The detailed mix ratio design is shown in Table 2. Based on the group's previous research (Liu et al., 2023a), it was found that introducing a high concentration of CO_2 gas (gas concentration >50%) would degrade foam quality, causing bubble fragmentation and gas escape. Based on trial tests, the CO_2 gas concentration was selected as 20%.

The foam volume was determined using the absolute volume method of admixture. To achieve the target density of 600 kg/m^3, 800 kg/m^3, and 1,000 kg/m^3, the selected admixture ratios were 55%, 40%, and 26%, respectively. Accordingly, the specimens were named S4-600, S4-800, and S4-1000. In addition, PP fiber was added to the specimen F1-600 with volume content of 1%. The effect of PP fiber reinforcement can be examined by comparing the mechanical performance of F1-600 to that of S4-600.

2.2 Specimen fabrication

The specimens were prepared using a homemade foaming drum, which consisted of a stirrer, a stirring drum, and a drum lid. The configuration of this drum can be found in the authors' previous research paper (Liu et al., 2023a). To ensure the airtightness of the foaming barrel, a sealing rubber ring was glued to the lid to prevent the escape of gas inside the barrel. The stirring net was welded onto the stirring rod to ensure that the blowing agent foams evenly within the stirring barrel. Small holes were left at the top and bottom of the mixing barrel wall for the foaming process. The bottom hole was used to fill the barrel with CO_2 gas (since CO_2 gas is denser than air). The top hole was equipped with a CO_2 concentration detector to monitor the CO_2 levels (with a detection range of 0%–100%). When the desired concentration was reached, the top and bottom holes were sealed to maintain a closed foaming environment.

According to the pre-set ratio, the cement, fly ash, and other dry powders were sifted to prevent aggregation that could hinder complete hydration. The materials were then weighed to match the design specifications. The weighed raw materials and PP fiber were poured into the mixer for 180 s of dry stirring to ensure uniform mixing. Water was added to form a slurry. Simultaneously, the hoof horn-type protein foamer and water were mixed at a 1:30 volume ratio and poured into the foaming bucket, which was then sealed with the lid. The gas valve was opened, and CO_2 gas was slowly introduced. When the CO_2 concentration detector indicated the set concentration, the valve was closed to stop the gas flow. The mixer was operated at 1800 r/min for 150 s to create a uniform foam with CO_2 gas encapsulated within it. The prepared foam was then added to the slurry and mixed thoroughly. The evenly mixed slurry was poured into molds and brushed with a release agent. The poured molds were covered with plastic wrap to minimize surface water evaporation. After 1 day, the molds were de-molded, and the specimens were transferred to the curing box for curing.

The side length of the cubic specimen was 70.7 mm, while the radius and height of the cylindrical specimen were 35 mm each. The specimens are shown in Figure 1.

2.3 Loading and measurement

The specimens cured for 3, 7, and 28 days were dried using a blast drying oven. The static compressive strength test of foam concrete cube specimens was carried out using a Sansi universal

FIGURE 2
Hopkinson lever system.

TABLE 2 Design of mixing ratios.

Specimen no.	Cement/kg	Fly ash/kg	Silica fume/kg	CO_2 concentration/vol%	PP fiber/kg	Water/kg	Foam mixing amount/%
S4-600	3.36	0.40	0.16	20	0	2.20	55
S4-800							40
S4-1000							26
F1-600					0.072	2.20	55

testing machine. Force-controlled loading was selected with a set rate of 0.01 MPa/s, and the average value of three specimens was taken for each set of test results.

The dynamic test was conducted using a Split Hopkinson Pressure Bar (SHPB) apparatus with a bar diameter of 75 mm. The high-pressure gas launching system operated within a pressure range of 0.2–4 MPa. The gun tube had a caliber of Φ75 mm and a length of 250 cm. The lengths of the impact bar, incident bar, and transmission bar were 50, 300, and 250 cm, respectively. Five different impact air pressures (0.08 MPa, 0.11 MPa, 0.14 MPa, 0.17 MPa, and 0.20 MPa) were set for the tests to ensure that the specimens were subjected to dynamic impact experiments under five different strain rates. The Hopkinson compression bar equipment is shown in Figure 2.

3 Test results and discussion

3.1 Static test results

Table 3 summarizes the tested functional and mechanical properties under static loading of the foam concrete. It can be seen that the strength of CO_2-cured foam concrete decreased significantly with the increase of foam volume admixture. The strength of 26% foam admixture was as high as 8.73 MPa, which was 32% higher than that of 40% foam admixture and 1.74 times higher than that of 55% foam admixture. Foam concrete is a porous cementitious material, and its compressive strength is primarily contributed by the pore walls. A lower volume of foam results in a higher concentration of pore walls and consequently higher compressive strength (Liu et al., 2023b). In comparison, the contribution of fiber reinforcement to static compressive strength was minimal.

3.2 Dynamic test specimen damage pattern

Before applying the impact loading using the SHPB device, the specimens were sandwiched intact between the incident and transmissive bars. After different air pressure impacts, the specimens were damaged to varying degrees. The failure morphology of different kinds of CO_2-cured foam concrete under different strain rates is shown in Figures 3–6.

Based on the figures, it was evident that the higher the strain rate, the more severe the overall damage and the greater the amount of powdery debris. Therefore, the degree of damage of CO_2-cured foam concrete was directly related to the strain rate. Under the action of a low strain rate (80 s^{-1}), the specimens split into larger fragments. As the strain rate gradually increased to 160 s^{-1}, the fragmentation became more severe, and both the size and number of fragments decreased. When the strain rate reached approximately 250 s^{-1}, the specimens were crushed, producing a significant amount of powdery debris. At a strain rate of 380 s^{-1}, the specimens were severely crushed, resulting in an increased number of powdery fragments and a decrease in the number of larger fragments.

In comparison, the CO_2-cured foam concrete with PP fiber reinforcement did not exhibit complete damage, especially at strain rates lower than 200 s^{-1}. Due to the bridging effect of the fibers, the foam concrete did not disintegrate into small, powdery pieces but remained connected in lumps.

3.3 Dynamic test data processing

The SHPB test needs to satisfy two fundamental assumptions: the one-dimensional stress wave assumption (planar assumption) and the stress uniformity assumption. The one-dimensional stress

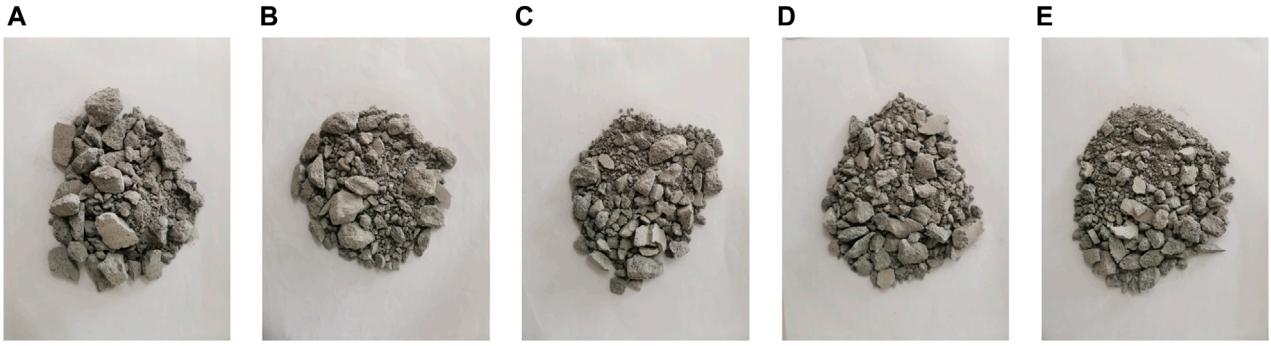

FIGURE 3
The failure pattern of 600 kg/m^3 CO_2 foam concrete: **(A)** 86 s^{-1}; **(B)** 176 s^{-1}; **(C)** 208 s^{-1}; **(D)** 247 s^{-1}; **(E)** 380 s^{-1}.

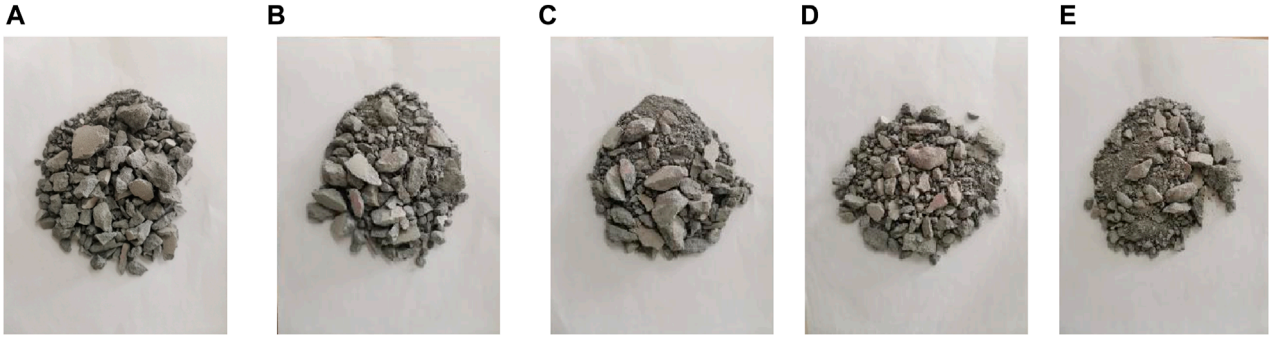

FIGURE 4
The failure pattern of 800 kg/m^3 CO_2 foam concrete: **(A)** 91 s^{-1}; **(B)** 172 s^{-1}; **(C)** 213 s^{-1}; **(D)** 255 s^{-1}; **(E)** 398 s^{-1}.

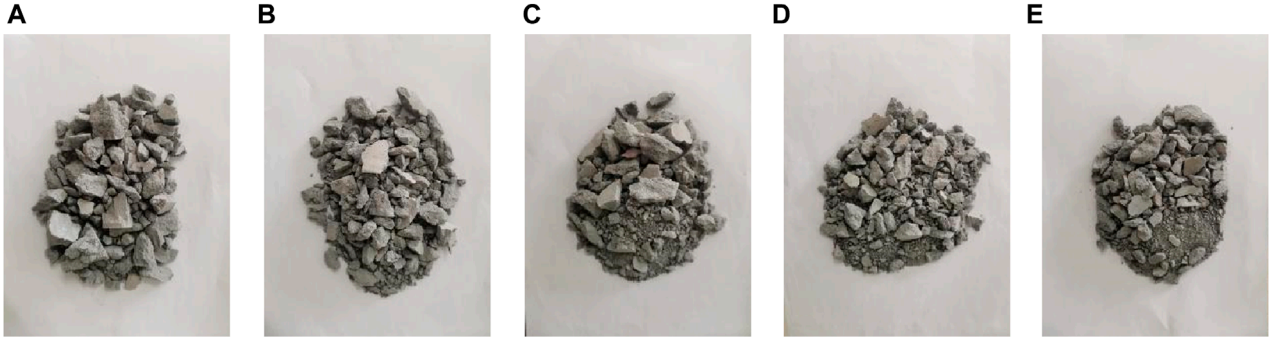

FIGURE 5
The failure pattern of 1,000 kg/m^3 CO_2 foam concrete: **(A)** 80 s^{-1}; **(B)** 163 s^{-1}; **(C)** 211 s^{-1}; **(D)** 242 s^{-1}; **(E)** 393 s^{-1}.

wave assumption requires that the stress pulse wave maintains a planar state across the cross-section of the bar during propagation. Typically, the bars are slender metallic rods made of isotropic materials, which satisfy the planar assumption when subjected to stress. The stress uniformity assumption states that the stress wave passes through the specimen multiple times, ensuring uniform stress distribution throughout the specimen. Usually, the wavelength of the stress wave is much greater than the length of the specimen, making it easier to meet this condition. The stress, strain, and strain rate of the material can be calculated using the following formulas

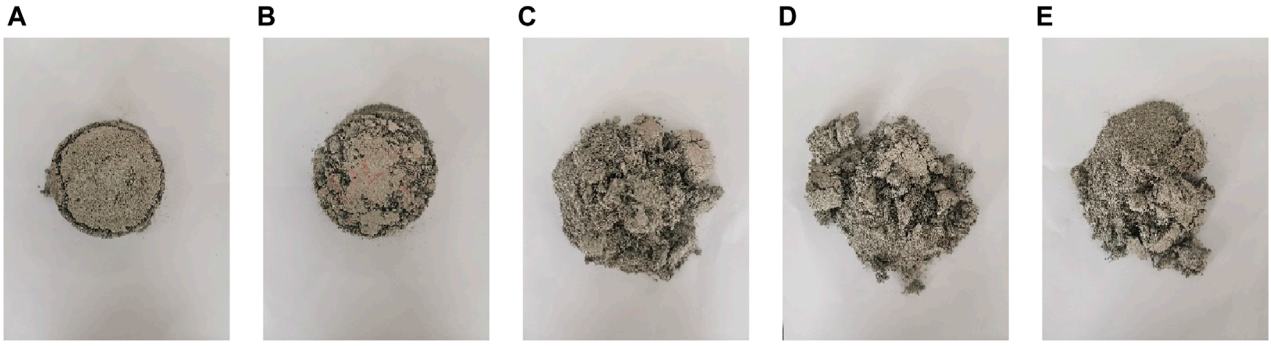

FIGURE 6
The failure pattern of 600 kg/m^3 CO_2 fiber foam concrete: **(A)** 89 s^{-1}; **(B)** 178 s^{-1}; **(C)** 217 s^{-1}; **(D)** 253 s^{-1}; **(E)** 397 s^{-1}.

(Zhao et al., 2019):

$$\dot{\varepsilon} = \frac{C_0}{L_s}\left[\varepsilon_i(t) - \varepsilon_r(t) - \varepsilon_t(t)\right] \tag{1}$$

$$\varepsilon = \frac{C_0}{L_s}\int_0^t \left[\varepsilon_i(t) - \varepsilon_r(t) - \varepsilon_t(t)\right]dt \tag{2}$$

$$\sigma = \frac{A_0}{2A_s}E_0\left[\varepsilon_i(t) + \varepsilon_r(t) + \varepsilon_t(t)\right] \tag{3}$$

Where E_0, C_0 are the elastic modulus of the compression bar and one-dimensional elastic wave velocity, respectively; $\varepsilon_i(t)$、$\varepsilon_r(t)$、$\varepsilon_t(t)$ are the incident pulse, reflected pulse, and transmitted pulse, respectively; A_0 is the cross-sectional area of the pressurized bar; A_s、L_s are the original cross-sectional area and length of the specimen, respectively.

It follows from the law of isotropy that the forces inside the specimen are the same (Zhu et al., 2009):

$$\varepsilon_i(t) + \varepsilon_r(t) = \varepsilon_t(t) \tag{4}$$

By substituting Eq. 4 into Eqs 1–3, the following equations can be obtained:

$$\dot{\varepsilon} = -\frac{2C_0}{L_s}\varepsilon_r(t) \tag{5}$$

$$\varepsilon = -\frac{2C_0}{L_s}\int_0^t \varepsilon_r(t)dt \tag{6}$$

$$\sigma = \frac{A_0}{A_s}E_0\varepsilon_t(t) \tag{7}$$

Equations 1–3, 5–7 are the three-wave and two-wave methods commonly used in analyzing SHPB experimental data. The data of this test were processed by the two-wave method. The strain rate, elastic modulus, dynamic compressive strength, and peak strain were calculated for different specimens under different impact air pressures. The dynamic stress increase factor DIF (dynamic increase factor) was utilized to describe the increase in compressive strength of the specimen under dynamic impact loading. The *DIF* can be determined using Eq. 8.

$$DIF = \frac{f_{cd}}{f_{cs}} \tag{8}$$

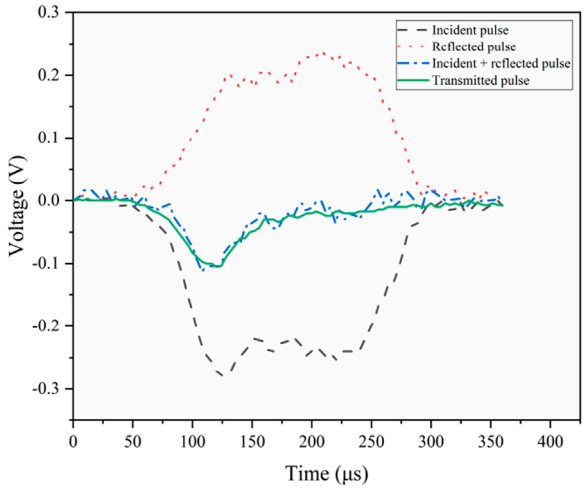

FIGURE 7
Stress balance verification.

Where: f_{cd} and f_{cs} are the dynamic compressive strength and static compressive strength of foamed concrete, respectively.

Please note that f_{cs} represents the cylinder compressive strength. Therefore, the cubic compressive strength obtained in this test was converted to the cylinder compressive strength by multiplying it by a coefficient of 0.8 (Kumavat and Patel, 2014).

To ensure the accuracy of the results obtained from the dynamic impact test, it was necessary to perform balance verification on the test results. A set of waveform curves was selected for one-dimensional stress wave balance verification, as shown in Figure 7. Rubber was used as a waveform shaper in the dynamic shock experiments. Probably due to the limited effect of rubber on waveform shaping, there is a high-frequency oscillation in some strain waves.

From the experimental waveform shown in Figure 7, it can be observed that the waveform rises smoothly and has a plateau segment. The waveform curve resulting from the superposition of the incident and reflected waves is essentially consistent with the waveform curve of the transmitted wave. This indicated that the specimen achieved a stress equilibrium state during the test.

TABLE 3 Properties of foam concrete.

Specimen no.	CO_2 concentration/vol%	Foam mixing amount/%	PP fiber/kg	Compressive strength/MPa			Peak strain	Dry density/kg/m^3
				3days	7 days	28 days		
S4-600	20	55	0	1.87	2.88	5.02	0.016	602
S4-800	20	40	0	2.25	3.91	6.62	0.021	813
S4-1000	20	26	0	3.39	5.20	8.73	0.019	1002
F1-600	20	55	0.072	1.98	3.01	5.07	0.009	605

Therefore, it can be concluded that the dynamic mechanical test results of CO_2-cured foam concrete under dynamic impact loading are accurate and reliable.

3.4 Dynamic stress-strain relationship

Based on the experimental data, the calculated dynamic mechanical properties of different types of CO_2 foam concrete at various strain rates are shown in Table 4. The strain rate was taken as the value of the plateau section when a plateau was present; otherwise, it was taken as the average value of the strain rate in the plastic phase (about 2/3 of the peak strain rate). The dynamic elastic modulus was determined from the approximately linear segment of the elastic phase of the stress-strain curve.

Figure 8 shows the determined dynamic stress-strain curves of four types of foam concrete with densities of 600, 800 and 1,000 kg/m^3 under strain rates ranging from 80 s^{-1}–380 s^{-1}. As illustrated, in the initial loading phase, the stress-strain relationship was generally linear, with the dynamic elastic modulus increasing as the strain rate increased. During this phase, the foam concrete pore walls bear the load, and the initial internal pore spaces remain intact, marking the linear elastic stage.

As the dynamic load increased, the weaker pore walls began to collapse under higher stress, and the specimen entered the yield stage, where plastic deformation started to occur. The locally collapsed pore walls were compacted and continued to bear the load, forming a stress plateau.

In the later loading stage, a large number of pore walls collapsed, and the compacted pore walls connected and broke, forming macroscopic fracture surfaces within the foam concrete specimen. The compressive strength of the specimen decreases rapidly. Once the pore structure of the foam concrete is completely destroyed, the specimen no longer bears any load.

Figure 8D demonstrates the dynamic stress-strain curves of CO_2-cured foam concrete with fiber reinforcements. It is evident that PP fiber reinforcement can effectively improve the dynamic mechanical properties and toughness of foam concrete. Specifically, PP fiber-reinforced specimens exhibited higher dynamic compressive strength and a longer plateau phase in the stress-strain curves compared to their unreinforced counterparts at the same density (Figure 8A). Additionally, the most significant enhancement in dynamic compressive strength due to fiber reinforcement was 17% at a strain rate of 210 s^{-1}.

3.5 The dynamic properties of foam concrete at different strain rates

To investigate the effect of strain rate on the dynamic properties of CO_2-cured foam concrete, the relationships between dynamic elastic modulus, dynamic compressive strength, DIF, and strain rate were specifically analyzed.

As shown in Figure 9, under the same density, the dynamic elastic modulus increased linearly with the increase in strain rate, demonstrating a clear strain rate dependence. As can be seen from Figure 9, for CO_2-cured foam concrete with a density of 600 kg/m^3, due to the large number of bubbles or pores contained within it, there was a buffering effect of these bubbles or pores when subjected to an external force, which reduced the degree of concentration of stress, thus slowing down the increase in the elastic modulus. As the density of the specimen increased, the slope of the dynamic elastic modulus fitting curve also increased gradually, and the increasing trend was more significant. For CO_2-cured foam concrete with a density of 1,000 kg/m^3, the dynamic elastic modulus reached 3.77 GPa under an impact load with a strain rate of 380 s^{-1}.

When the strain rate increased, the stress transfer and response speed inside the material would be accelerated. However, it took a certain amount of time for cracks to develop and expand, and the strain could not immediately keep up with the change in stress, and there was a delay effect. This delay effect of the expansion rate would make the strain smaller under the same stress condition (Wang et al., 2012).

As shown in Figure 10, the dynamic compressive strength increased linearly with the strain rate at the same density. For CO_2-cured foam concrete containing a large number of pores and microcracks, the damage mechanism was mainly influenced by the generation and expansion of cracks inside the material under external loading. Under high strain rate conditions, foam concrete was subjected to rapid loading and its internal stress state changes rapidly. Due to the pores and microcracks in the material, the stress concentration phenomenon was more significant, leading to the accelerated generation and expansion of cracks. The formation and expansion of these cracks required energy consumption. Therefore, as the strain rate increases, the number of cracks produced increases and so does the amount of energy required. However, due to the instantaneous nature of the impact, the material did not have enough time to accumulate energy through deformation or otherwise to cope with the external impact. To counteract this external energy, the material could only respond by increasing the stress. Therefore, as the strain rate increased, the dynamic compressive strength

TABLE 4 Dynamic mechanical property parameters of CO_2 fiber foam concrete.

Specimen no.	Density (kg/m^3)	Strain rate (s^{-1})	Elastic modulus (GPa)	Peak stress (MPa)	Peak strain	DIF
S4-600-1	605	380	0.45	9.49	0.134	2.363
S4-600-2	603	247	0.35	8.81	0.130	2.194
S4-600-3	601	208	0.31	7.58	0.060	1.889
S4-600-4	611	176	0.28	6.78	0.110	1.688
S4-600-5	603	86	0.24	6.18	0.059	1.538
S4-800-1	813	398	0.9	13.00	0.058	2.455
S4-800-2	802	255	0.62	11.20	0.054	2.115
S4-800–3	803	213	0.51	10.50	0.074	1.983
S4-800-4	800	172	0.47	9.06	0.054	1.711
S4-800-5	805	91	0.44	7.87	0.087	1.486
S4-1000-1	1009	383	3.77	16.94	0.050	2.425
S4-1000-2	1003	242	2.71	15.13	0.038	2.166
S4-1000-3	1001	211	2.46	13.80	0.037	1.976
S4-1000-4	997	163	1.85	12.54	0.041	1.795
S4-1000-5	1005	80	1.23	10.99	0.037	1.574
F1-600-1	602	397	0.52	10.064	0.106	2.481
F1-600-2	608	253	0.45	9.385	0.128	2.313
F1-600-3	613	217	0.37	8.482	0.141	2.091
F1-600-4	601	178	0.30	7.833	0.091	1.931
F1-600-5	598	89	0.27	6.794	0.110	1.675

increased accordingly in response to more rapid loading and higher energy input.

The strain rate sensitivity of CO_2-cured foam concrete was closely related to the combination of its internal crack propagation path and velocity. As can be seen from Figure 11, DIF increased almost linearly with the logarithm of strain rate, showing an obvious strain rate enhancement effect. The correlation between the logarithm of strain rate ($\dot{\varepsilon}$) and the DIF can be generally described by the following equations:

$$DIF = 1.59 \times lg(\dot{\varepsilon}) - 2.17 \,(\mathrm{S4-600}) \tag{9}$$

$$DIF = 1.58 \times lg(\dot{\varepsilon}) - 2.14 \,(\mathrm{S4-800}) \tag{10}$$

$$DIF = 1.37 \times lg(\dot{\varepsilon}) - 1.58 \,(\mathrm{S4-1000}) \tag{11}$$

In Eqs 9–11, the strain rate applies in a range from 150 s^{-1} to 400 s^{-1}. At high strain rates, the crack propagation and interactions within the material become particularly complex. Since CO_2-cured foam concrete has a porous structure, these pores may become the starting point or channel for crack extension during dynamic loading, affecting the crack propagation path (Deng et al., 2016). Meanwhile, the crack propagation rate was affected by the strain rate. At high strain rates, the crack propagation speed was accelerated, which may lead to more cracks forming and expanding in a shorter time. This rapid crack propagation and interaction further enhanced the dynamic response of the material, which was manifested as an increase in the DIF value.

3.6 The dynamic properties of foam concrete at different densities

This section analyzes the impact of different foam volume admixtures on the dynamic properties of foam concrete with varying densities, including the relationships between dynamic

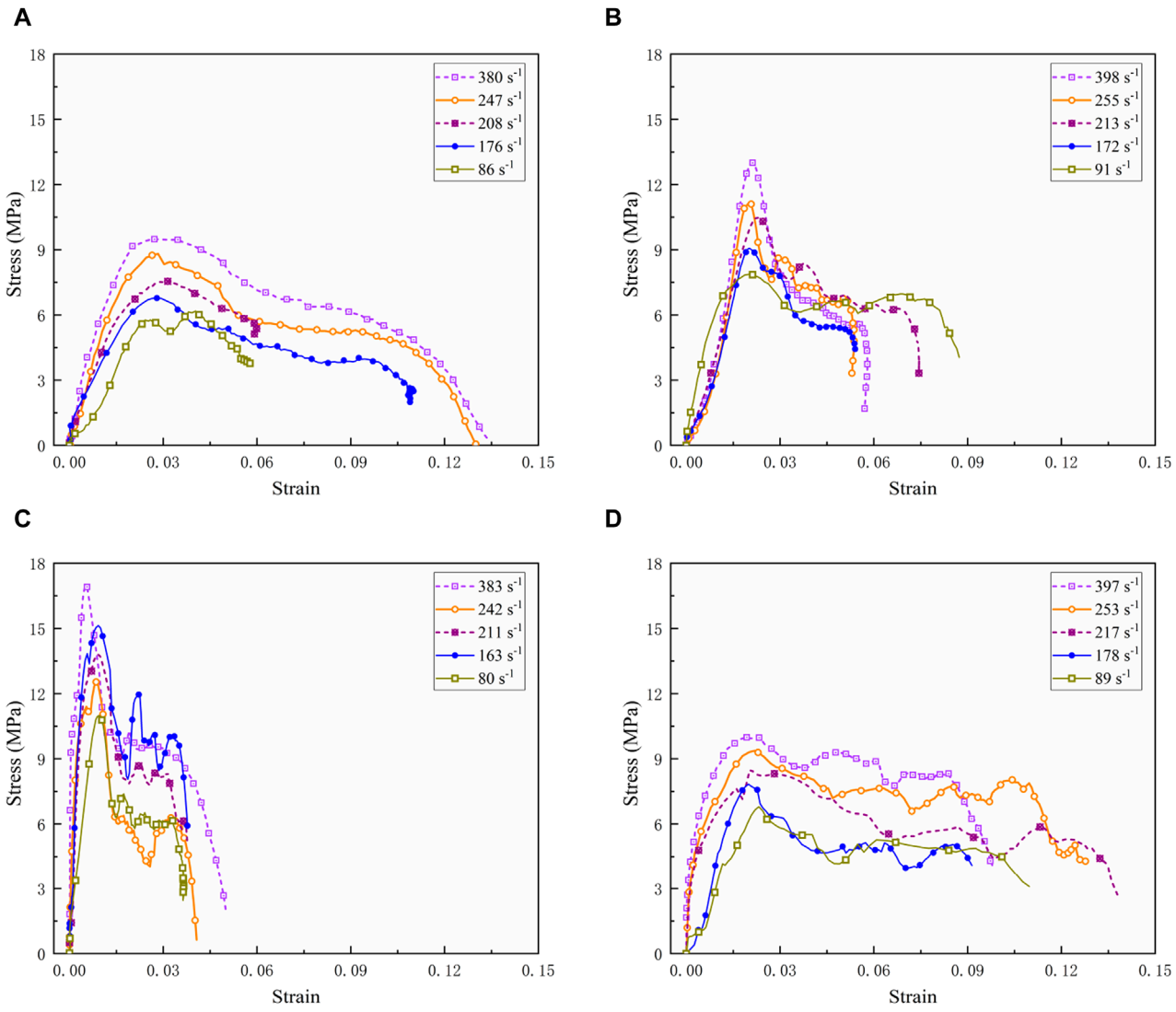

FIGURE 8
Dynamic stress-strain curves of CO_2 fiber foamed concrete under different strain rate loadings: **(A)** ρ = 600 kg/m^3; **(B)** ρ = 800 kg/m^3; **(C)** ρ = 1,000 kg/m^3; **(D)** ρ = 600 kg/m^3 fiber.

elastic modulus, dynamic compressive strength, DIF, and density. The relationship between dynamic elastic modulus and density is shown in Figure 12.

As shown in Figure 12, at a given strain rate, the dynamic elastic modulus increased as a power function with increasing density, indicating a significant density dependency for CO_2-cured foam concrete. The variation of dynamic elastic modulus at increasing density can be generally described using the (Eqs 12–16):

$$E = 3.7 \times 10^{-18} \times D^6 \left(\dot{\varepsilon} = 380^{-1}\right) \quad (12)$$

$$E = 2.6 \times 10^{-18} \times D^6 \left(\dot{\varepsilon} = 240^{-1}\right) \quad (13)$$

$$E = 5.0 \times 10^{-19} \times D^6 \left(\dot{\varepsilon} = 210^{-1}\right) \quad (14)$$

$$E = 6.3 \times 10^{-17} \times D^5 \left(\dot{\varepsilon} = 160^{-1}\right) \quad (15)$$

$$E = 1.1 \times 10^{-12} \times D^4 \left(\dot{\varepsilon} = 80^{-1}\right) \quad (16)$$

At higher densities, the internal porosity was smaller and the pore walls between pores were thicker, causing a stronger delay in crack propagation. Therefore, the dynamic elastic modulus increased significantly with increasing density.

Figure 13 shows the relationship between density and dynamic compressive strength. As can be seen from the figure, there was a significant positive correlation between the dynamic compressive strength and the density of CO_2-cured foam concrete. At the same strain rate, as the density increases, the dynamic compressive strength increases accordingly, and this relationship exhibits a linear trend.

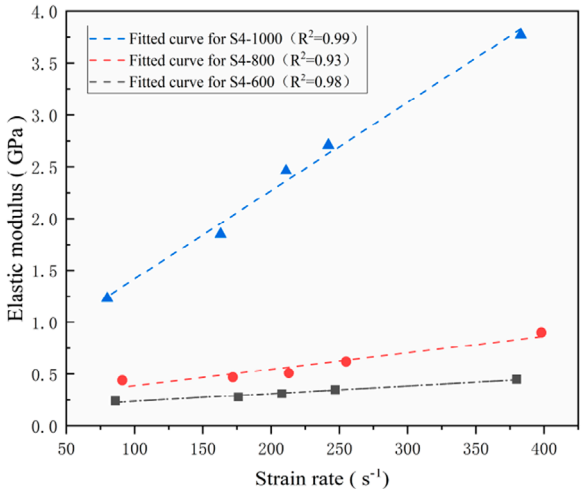

FIGURE 9
Dynamic elastic modulus *versus* strain rate.

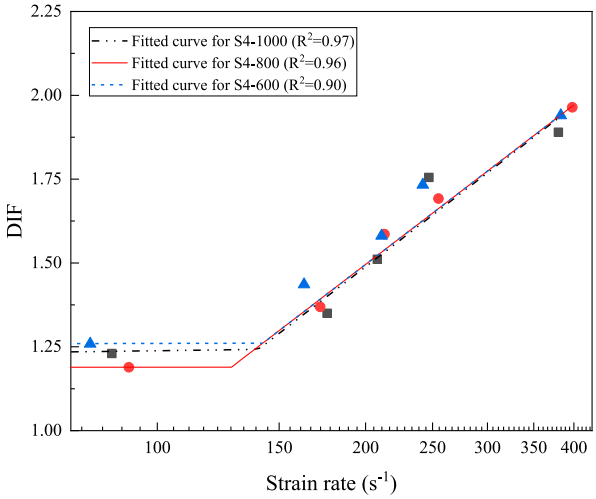

FIGURE 11
DIF *versus* strain rate.

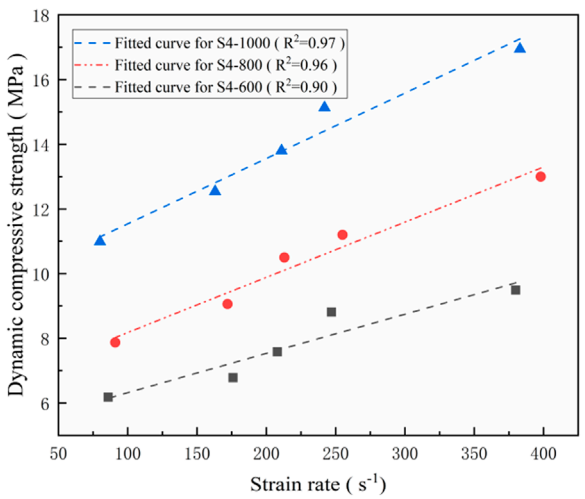

FIGURE 10
Dynamic compressive strength *versus* strain rate.

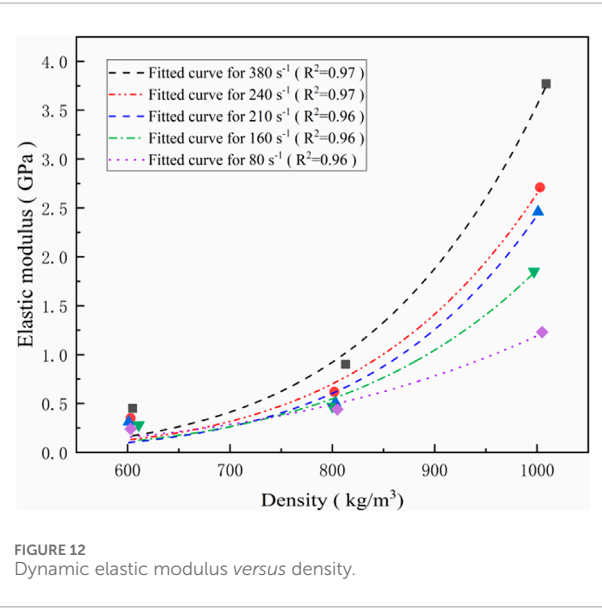

FIGURE 12
Dynamic elastic modulus *versus* density.

In the strain rate range of 160 s^{-1}–240 s^{-1}, the relationship between dynamic compressive strength and density is particularly pronounced, showing an approximately increasing trend. This indicated that within this strain rate range, the stress transmission and response speed inside the material matched the external loading speed, making the density variation have a more direct impact on the material's mechanical behavior. Additionally, as the density increased, the differences in dynamic compressive strength under five different strain rate loads became more apparent. This meant that changes in density not only affected the overall impact resistance of the material but also influenced its performance under different strain rates.

Figure 14 shows the relationship between the density of CO_2-cured foam concrete and the DIF value. As shown in the figure, the DIF value of specimens exhibited different trends related to density at various strain rates. Under lower strain rates (80 s^{-1}), the DIF value remained almost constant with increasing density. This may be because, at low strain rates, the stress transmission and response speed within the material was relatively slow, insufficient to cause significant dynamic effects.

When the strain rate exceeded 100 s^{-1}, the DIF value began to change with increasing density. This indicated that at higher strain rates, changes in density significantly affected the material's dynamic performance. At high strain rates, the stress state within the material changes more drastically, and materials with different densities exhibit different dynamic response characteristics when coping with these rapidly changing stress states.

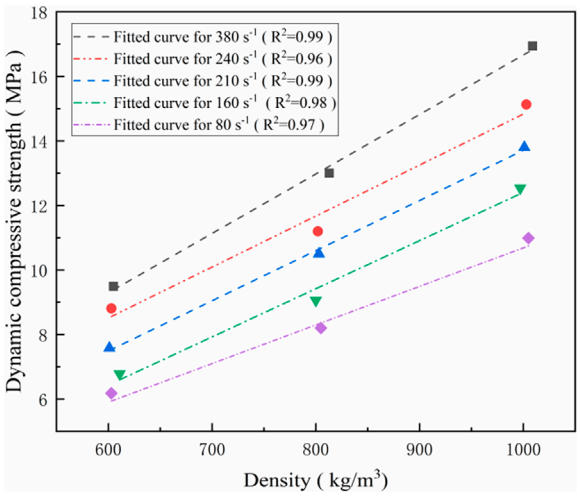

FIGURE 13
Dynamic compressive strength *versus* density.

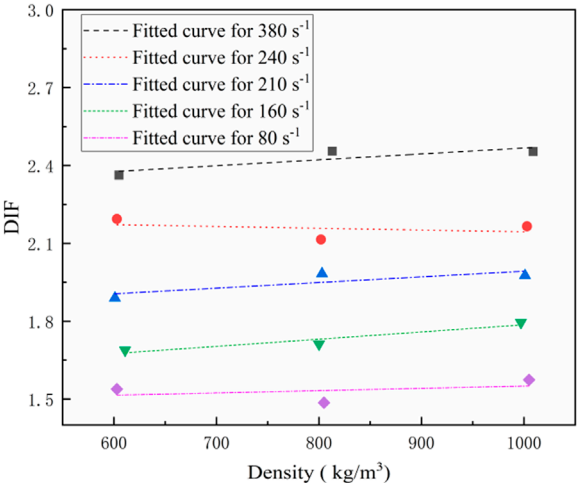

FIGURE 14
DIF *versus* density.

4 Conclusion

In this paper, experimental explorations were conducted to investigate the effect of foam admixture and the addition of fibers on the performance of CO_2-cured foam concrete. Based on the above results and discussions, the following conclusions can be drawn.

(1) The addition of PP fibers can effectively improve the dynamic properties of CO_2-cured foam concrete, including compressive strength and toughness, while its impact on the static properties is minimal.
(2) At the same strain rate, the dynamic elastic modulus increases as a power function of density, indicating that CO_2-cured foam concrete has a significant density dependence. It is because the delayed response to dynamic cracking was more pronounced at higher density CO_2-cured foam concrete.
(3) The dynamic compressive strength increases almost linearly with density under similar strain rates. The enhancement in dynamic compressive strength at increasing densities tends to be more pronounced at higher loading rates.
(4) At low strain rates, the variation in DIF value at different densities is not significant; however, it becomes obvious at higher strain rates.
(5) The dynamic elastic modulus of CO_2-cured foam concrete increases almost linearly with the increasing strain rate, demonstrating a clear strain rate-dependence.

Data availability statement

The original contributions presented in the study are included in the article/Supplementary Material, further inquiries can be directed to the corresponding author.

Author contributions

YL: Conceptualization, Writing–review and editing. SH: Methodology, Writing–original draft. JF: Project administration, Writing–review and editing. TS: Funding acquisition, Project administration, Writing–review and editing. DG: Supervision, Validation, Writing–review and editing.

Funding

The author(s) declare that financial support was received for the research, authorship, and/or publication of this article. The authors would like to acknowledge the financial support received from National Natural Science Foundation of China (52278236, 52172013, and 51478406), Anhui Provincial Universities Natural Science Research Project (KJ2020ZD43, 2022AH050261), Anhui Provincial Natural Science Foundation Project (1908085ME144), and Doctoral Startup Foundation from Anhui Jianzhu University (2022QDZ23), the Department of Science and Technology of Guangdong Province, China (2023A1515110842), the open Foundation of the Key lab of Prefabricated Building Research Institute of Anhui Province (AHZPY2023KF02), and Anhui Jianzhu University Ph. D Foundation (2019QDZ29). Anhui Provincial Teaching Research Project, grant number 2020jyxm0347; Anhui Institute of Building Research & Design, grant number AHZPY20201KF.

Conflict of interest

TS was employed by China Construction Third Bureau First Engineering Co., Ltd.

The remaining authors declare that the research was conducted in the absence of any commercial or financial relationships that could be construed as a potential conflict of interest.

Publisher's note

References

Blanc, L., Schunck, T., and Eckenfels, D. (2021). Sacrificial cladding with brittle materials for blast protection. *Materials* 14, 3980. doi:10.3390/ma14143980

Deng, J., Qin, Y., Li, X., and Zhu, M. (2024). Investigation of the CFRP-concrete interfacial performance under adhesive curing using the PZT-based wave propagation technique. *Constr. Build. Mater.* 418, 135375. doi:10.1016/j.conbuildmat.2024.135375

Deng, Z., Cheng, H., Wang, Z., Zhu, G., and Zhong, H. (2016). Compressive behavior of the cellular concrete utilizing millimeter-size spherical saturated SAP under high strain-rate loading. *Constr. Build. Mater.* 119, 96–106. doi:10.1016/j.conbuildmat.2016.05.018

Feng, S., Zhou, Y., and Li, Q. M. (2022). Damage behavior and energy absorption characteristics of foamed concrete under dynamic load. *Constr. Build. Mater.* 357, 129340. doi:10.1016/j.conbuildmat.2022.129340

Feng, S., Zhou, Y., Wang, Y., and Lei, M. (2020). Experimental research on the dynamic mechanical properties and damage characteristics of lightweight foamed concrete under impact loading. *Int. J. Impact Eng.* 140, 103558. doi:10.1016/j.ijimpeng.2020.103558

Gökçe, H. S., Öksüzer, N. U., Kamiloğlu, H. A., Eyüboğlu, M., and Yılmaz, F. (2023). The toughness of polypropylene fiber-reinforced foam concrete under various uni-and tri-axial compression loads. *KSCE J. Civ. Eng.* 27, 2982–2992. doi:10.1007/s12205-023-1345-9

Guo, D., Gao, W.-Y., and Dai, J. G. (2022). Effects of temperature variation on intermediate crack-induced debonding and stress intensity factor in FRP-retrofitted cracked steel beams: an analytical study. *Compos Struct.* 279, 114776. doi:10.1016/j.compstruct.2021.114776

Guo, D., Gao, W. Y., Liu, Y. L., and Dai, J. G. (2023). Intermediate crack-induced debonding in CFRP-retrofitted notched steel beams at different service temperatures: experimental test and finite element modeling. *Compos. Struct.* 304, 116388. doi:10.1016/j.compstruct.2022.116388

Guo, Q., Gou, Y., Chen, J., Zhang, Y., and Zhou, Y. (2020). Dynamic response of foam concrete under low-velocity impact: experiments and numerical simulation. *Int. J. Impact Eng.* 146, 103693. doi:10.1016/j.ijimpeng.2020.103693

He, Y., Gao, M., Zhao, H., and Zhao, Y. (2019). Behaviour of foam concrete under impact loading based on SHPB experiments. *Shock Vib.* 2019, 1–13. doi:10.1155/2019/2065845

Huang, H. J., Gong, N. P., Mu, C. M., Zhou, H., and Liu, W. (2020). Dynamic mechanical properties and constitutive relation of foam concrete. *J. Build. Mater.* 23, 466–472.

Kumavat, H. R., and Patel, V. J. (2014). Factors influencing the strength relationship of concrete cube and standard cylinder. *Int. J. Innovative Technol. Explor. Eng.* 3, 76–79.

Li, F. X., Li, J. X., Xiao, M., and Ren, M. M. (2022). Impact resistance of lightweight steel-framed foamed concrete composite wall panels. *Build. Chin. Ceram. Soc.* 41, 68–75.

Liu, F., Zhao, K., Wang, X. J., and Ren, H. Q. (2007). A study on SHPB method of soft/porous materials. *J. Exp. Mech.* 22, 7.

Liu, Y. L., Li, C. F., Zhai, H. X., Ahmad, M. R., Guo, D., and Dai, J. G. (2023a). Production and performance of CO2 modified foam concrete. *Constr. Build. Mater.* 389, 131671. doi:10.1016/j.conbuildmat.2023.131671

Liu, Y. L., Liu, C., Qian, L. P., Wang, A. G., Sun, D. S., and Guo, D. (2023b). Foaming processes and properties of geopolymer foam concrete: effect of the activator. *Constr. Build. Mater.* 391, 131830. doi:10.1016/j.conbuildmat.2023.131830

Lu, L. G., Xu, Y., Ge, J. J., Yao, W., and Gu, K. K. (2022). Dynamic mechanics and energy characteristics of foamed concrete with different rubber content. *Concrete* 09, 6–10.

Ma, Z., Ma, C., Du, C., Zhang, S., Zhang, H., Zhang, X., et al. (2023). Research on dynamic mechanical properties of polypropylene fiber-modified rubber foamed concrete. *Constr. Build. Mater.* 404, 133282. doi:10.1016/j.conbuildmat.2023.133282

Rostami, V., Shao, Y., Boyd, A. J., and He, Z. (2012). Microstructure of cement paste subject to early carbonation curing. *Cem. Concr. Res.* 42, 186–193. doi:10.1016/j.cemconres.2011.09.010

Shi, C., He, F., and Wu, Y. (2012). Effect of pre-conditioning on CO2 curing of lightweight concrete blocks mixtures. *Constr. Build. Mater.* 26, 257–267. doi:10.1016/j.conbuildmat.2011.06.020

Shi, C. J., Wang, J. Y., Tu, Z. J., and Wang, D. H. (2017). Progresses in CO2 curing of concrete. *Mater. Rep.* 31, 134–138.

Wang, J. G., Gao, Q. C., Lu, H., Liang, S. F., Huang, B., and Yang, Z. (2015). Impact response tests of layered medium with SHPB. *J. Vib. shock* 34, 192–197.

Wang, S., Zhang, M. H., and Quek, S. T. (2012). Mechanical behavior of fiber-reinforced high-strength concrete subjected to high strain-rate compressive loading. *Constr. Build. Mater.* 31, 1–11. doi:10.1016/j.conbuildmat.2011.12.083

Wang, X., Liu, L., Shen, W., and Zhou, H. (2019). CFRP reinforced foam concrete subjected to dynamic compression at medium strain rate. *Materials* 13, 10. doi:10.3390/ma13010010

Wang, X., Zhang, X., Song, L., Zhou, H., Wang, Y., Zhang, H., et al. (2021). Mitigating confined blast response of buried steel box structure with foam concrete. *Thin-Walled Struct.* 169, 108473. doi:10.1016/j.tws.2021.108473

Yan, Z. W., Bai, Y. L., Ozbakkaloglu, T., Gao, W. Y., and Zeng, J. J. (2021). Rate-dependent compressive behavior of concrete confined with Large-Rupture-Strain (LRS) FRP. *Compos. Struct.* 272, 114199. doi:10.1016/j.compstruct.2021.114199

Yang, J., Chen, J. W., Qin, P., Huang, J. F., He, B., and Li, Y. J. (2020). Experiment study on impact resistance of foam concrete superimposed wallboard. *New Build. Mater.* 47, 81–85.

Zhao, X., Xu, S., Li, Q., and Chen, B. (2019). Coupled effects of high temperature and strain rate on compressive properties of hybrid fiber UHTCC. *Mater. Struct.* 52, 92–17. doi:10.1617/s11527-019-1391-4

Zheng, L., and Jones, M. R. (2013). Energy absorption of foamed concrete from low-velocity impacts. *Mag. Concr. Res.* 65, 209–219. doi:10.1680/macr.12.00054

Zhu, J., Hu, S., and Wang, L. (2009). An analysis of stress uniformity for concrete-like specimens during SHPB tests. *Int. J. Impact Eng.* 36, 61–72. doi:10.1016/j.ijimpeng.2008.04.007